ACS APPLIED POLYMER MATERIALS

pubs.acs.org/acsapm

Article

Consequences of Humidity Cycling on the Moisture Absorption Characteristics of Epoxy Resins with Different Network Architectures

Rishabh D. Guha, Evgeny O. Danilov, Katherine Berkowitz, Oluwatimilehin Oluwajire, and Landon R. Grace*

Cite This: *ACS Appl. Polym. Mater.* 2023, 5, 400−411

Read Online

ACCESS | Metrics & More | Article Recommendations | Supporting Information

ABSTRACT: Absorbed moisture is a perpetual contributor to the steady loss of performance for in-service epoxy-based polymer materials. On the atomistic scale, the state of individual water molecules in a crosslinked epoxy is dependent on the strength of the secondary bonding interactions they engage in and their local physical environment. However, these chemical and physical variables can be tailored on the macroscopic scale through changes in the experimental curing schedule. In this study, crosslinked epoxy matrices with different network architectures were cured by varying the stoichiometric mixing ratios of the epoxy: hardener combination. The samples were subsequently subjected to fluctuating humidity conditions which comprises repeating cycles of high (∼95% RH) and ambient humidity. Both infrared (IR) spectroscopy and dielectric readings were successful in establishing a strong correlation between moisture absorption, network morphology, and dielectric properties. An anomalous behavior observed during the spectral peak analysis helped us understand how absorption history can redistribute the concentrations of water species at the same moisture concentrations. The results from this study elucidate how the phenomenon of absorption itself can act as a damage initiation event, and they also indicate that the spatial quantification of the different water species across a sample can allow us to map damage sites, nanopores, and areas with an overall higher void content.

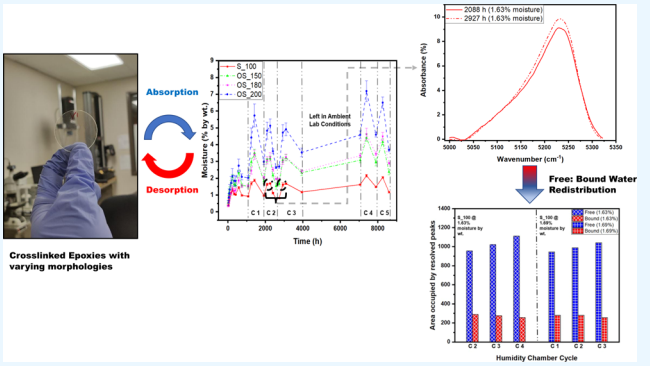

KEYWORDS: *epoxy, moisture, humidity, infrared spectroscopy, dielectric properties*

1. INTRODUCTION

The continuous demand for improved performance in engineering applications has created a global composite market which is expected to be evaluated at 146.14 billion USD in 2026.[1] A higher strength-to-weight ratio,[2] resistance to chemical contamination,[3] and thermal stability[4] are a few properties which have propelled its widespread adoption over conventional materials in safety-critical structures such as aircraft, automobiles, and marine assemblies, frequently operating in extreme environments.[5] The polymeric matrix used in a composite holds the reinforcing fibers together, transfers stress between them, and protects the fibers from mechanical and environmental damage.[6] For high-performance composites, epoxy resins have been widely studied as a matrix material over the years.[7] It has been found that they offer a great combination of strength and durability, making them a primary candidate for composite matrices. Despite the favorable properties, the polar nature of the epoxy matrix makes these crosslinked polymeric networks highly susceptible to atmospheric moisture absorption even in low-humidity operating conditions.[2,5,8] Neat epoxy-based resins can absorb anywhere between 1 and 7% moisture by wt.[9] which can translate to a moisture content of ∼3% by wt.[10] in a polymer composite. The penetrant water molecules fundamentally alter the chemical architecture of the crosslinked epoxy and lower its glass transition temperature (T_g).[11,12] Consequently, there is a significant degradation in the thermal and electrical insulation properties of the matrix.[5] The absorbed moisture also causes matrix plasticization which has a direct impact on the mechanical properties and the overall service life of the composite structure.[13] The repetitive cycles of moisture absorption−desorption inadvertently imposed by the rapidly fluctuating humidity conditions can also act as damage initiation events through swelling-induced nanovoids, pores, and microcracks.[14,15]

Different characterization techniques and experimental strategies which include long-term gravimetric uptake stud-

Received: September 9, 2022
Accepted: December 20, 2022
Published: January 3, 2023

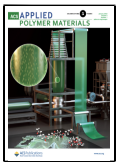

ies,[16,17] nuclear magnetic resonance spectroscopy,[18] dielectric relaxation spectroscopy (DRS),[19−21] and medium/near-infrared (MIR/NIR) spectroscopy[22−26] have been employed over the years to understand the intermolecular interactions which govern the phenomena of moisture absorption and transport in an epoxy resin. A common thread running through the conclusions of all these investigations is that the state of moisture after absorption is dictated by both the secondary chemical interactions (hydrogen bonding, van der Waals, and dispersion forces) and the local physical environment. Absorbed water molecules close to polar atoms in the matrix engage in strong intermolecular hydrogen bonding, while water molecules residing in microcracks, nanopores, and voids are less firmly bound to the polymer chain, existing as clusters of "free" water.[27] In recent times, in silico studies have corroborated this dual nature of absorbed water by comparing the trends of intermolecular secondary bonding interactions as a function of polarity, temperature, network morphology, and the presence of interfacial damage sites.[28−34]

Experimental identification and subsequent quantification of these different species for the same chemical constituent (water) is particularly challenging, but as evidenced in the studies by Musto[23,24] and Herrera-Gómez,[22] NIR spectroscopy can be effectively leveraged for this application in extensively hydrogen-bonded molecular structures like a moisture-contaminated crosslinked epoxy. In the NIR spectral band of 780−2500 nm, the absorption peaks are either multiples or overtone combinations of the peaks from the MIR region.[24] The improved resolution in the −OH vibrational stretching and deformation (ν_{OH}) makes it possible to separate out the contributions of the individual water species and quantify their respective concentrations. The "free" and "bound" water species also have specific responses under the influence of an electromagnetic field.[35,36] The split postdielectric resonator (SPDR) can be used to leverage this phenomenon and measure the relative permittivity of absorbed moisture as it chemically interacts with the polymer network.[8,25,37,38] Within the 1−10 GHz range, the dipolar contributions of molecules dominate, and characteristic dipoles such as water can rotate freely with the changing electromagnetic field.[39] However, the water molecules engaging in secondary bonding interactions with the polymer network are considerably more restricted in their ability to rotate and align themselves to the oscillating field.[40] On the other hand, the "free" water molecules existing in microcracks and voids exhibit dielectric characteristics which are similar to bulk water. Consequently, the relative permittivity of free water within this frequency range is much higher (∼80)[36] compared to that of firmly bound water (∼3).[5,39] The analysis of the differences in relative permittivities measured at different moisture concentrations can also allow us to gain some insight into the uptake characteristics of epoxy resins with different chemical morphologies.

Multiple experimental investigations have been performed over the past decades which have tried to isolate the individual roles of topology and polar interactions on thermomechanical properties[31,41,42] or on the more elusive and poorly understood topic of moisture absorption.[9,43,44] Different approaches have been used to alter the network architecture which include tuning the mixing ratios of epoxy: hardener,[45,46] using multiple cyclic/aliphatic formulations,[47,48] or adding chemical fillers and modifiers of varying shapes and sizes.[49,50] Stoichiometric ratios of epoxy and the hardener, followed by the optimal curing schedule, create matrices with the maximum possible degree of crosslinking, but studies have shown that both under-stoichiometric and over-stoichiometric mixing ratios[51] reduce the crosslinking density. Moreover, over-stoichiometric concentrations of the hardener increase the available polar sites which in turn influences the hydrogen bonding (H-bonding) network created between the matrix and the moisture absorbed during exposure.

In our previous works, we analyzed the influence of polarity and network topology on the nonbonded secondary interactions between absorbed moisture and an epoxy polymer matrix.[29,30] These investigations were made possible by in silico studies where we could explicitly control the number of crosslinking reactions by stopping the iterative algorithm at different time steps. On the atomistic scale, this produced polymer networks with fundamental differences in the degree of crosslinking, available free volume, and concentration of polar sites without any change in stoichiometry. This degree of local control is not available in experiments. Varying the stoichiometric mixing ratios of the reactants is a feasible route to control the crosslinking density and validate the molecular-level takeaways on the macroscopic scale. The change in stoichiometry during the experimental curing schedule produces polymer matrices with different architectures which could then be eventually subjected to a common and consistent moisture absorption regime. Polymer matrices were cured by fixing the concentration of the diglycidyl ether of bisphenol A (DGEBA) epoxy and varying the added amounts of the diethylene triamine (DETA) hardener. Four classes of such epoxies were cured, and the physical properties were validated through a thermomechanical analysis on the dynamic mechanical analysis (DMA). Subsequently, they were exposed to the same ambient conditions, and the changes in the rate and extent of absorption in these different classes were monitored by the gravimetric uptake profiles. The differences in the moisture absorption characteristics in these epoxy resins were analyzed through periodic readings on a NIR spectrophotometer and SPDR. The strong influence of subtle changes in humidity on the absorption behavior was identified at the beginning of the uptake profile, and subsequently, the effects of humidity cycling were also incorporated into the exposure regime. The over-stoichiometric epoxy networks with higher polarity and lower crosslinking density consistently absorbed more moisture than the stoichiometric matrix. The quantitative differences in moisture absorption for the different epoxy classes were almost linearly tracked by the characteristic moisture peak area in the NIR spectra and the changes in dielectric constants recorded by the SPDR. The relative concentrations of the free and bound water species were evaluated by deconvoluting the spectral characteristic NIR peak into resolved components. An anomalous trend was observed during the deconvolution of the characteristic peak as identical moisture concentrations were found to have different component peak heights. Further investigations of this behavior led us to the conclusion that absorption induces matrix swelling and generates additional free volume. Future cycles of absorption preceded by desorption redistribute the relative concentrations of the free and bound water species and allow more water to exist in the free state in these moisture-induced voids and cracks.

https://doi.org/10.1021/acsapm.2c01570
ACS Appl. Polym. Mater. 2023, 5, 400−411

2. MATERIALS AND METHODS

2.1. Materials. The polymer networks analyzed in this work were prepared from different stoichiometric combinations of an epoxy and hardener. DER 332, supplied by Sigma-Aldrich, was used as the epoxy resin. Chemically, the resin is very close to the pure DGEBA and has a molar mass of 340.41 g/mol. The chemical structure of the epoxy is depicted in Figure 1a. We can observe the two available epoxide rings

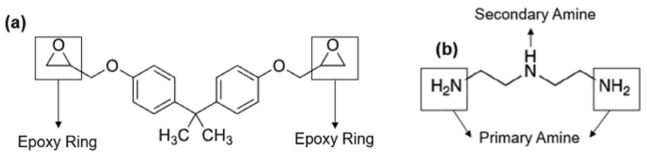

Figure 1. Chemical structure of the (a) DGEBA epoxy and (b) DETA hardener.

in the compound, which translates to an epoxy equivalent molar mass of ∼170 g/mol. The hardener used for the curing process was DETA, from Alfa Aesar with a labeled purity of 99.0%. This hardener is an aliphatic amine with a molar mass of 103.14 g/mol. As seen in Figure 1b, the compound is constituted of two primary amine sites and one secondary amine site.

2.2. Sample Preparation. It has been reported in previous studies that the nonstoichiometric ratios of the hardener added during the curing process influence the crosslinking density of the resultant polymer network.[51] Vaughan *et al.*[52] found that deviations to either side of the stoichiometric ratio reduce the T_g of the polymer with the decrease being sharper in under-stoichiometric mixtures. However, under-stoichiometric ratios tend to not cure into resilient solids. In the dissertation by Brockmann,[53] it was discussed that there is a particular sequence in which the amine groups of the DETA react with the DGEBA molecules. An excess of the hardener generates an increased number of free chain ends consisting of incompletely saturated DETA molecules. Therefore, over-stoichiometric amounts of the hardener create a more flexible network with lower crosslinking density. In case of an extreme excess of DETA, the molecules might remain completely unreacted with the epoxy molecules and act as plasticizers in the polymer.[54] The approach of using over-stoichiometric ratios during curing has been previously adopted in multiple studies to vary the network structure.[46,52,55] Since this work investigates the effect of moisture absorption and the intermolecular network−water interactions, it is worth noting that an excess concentration of the hardener will increase the number of polar amine sites. Consequently, over-stoichiometric mixtures will have a combined effect of higher polarity and additional free volume created due to a reduced crosslinking density. For this study, four different classes of samples were cured starting from the stoichiometric ratio. In the remaining three classes, the hardener proportion was modified as a percentage of the stoichiometric hardener mass ratio. The percentage of the hardener used, epoxy to hardener mass distribution, and the names given to the individual classes of samples have been summarized in Table 1.

The samples were prepared by pouring the uncured epoxy into a vacuum beaker. Then, the appropriate concentration of the hardener for a particular class of sample was poured into the beaker using a steel funnel. Initially, the mixture was viscous, and it was manually stirred using a stainless-steel spatula. When the mixture viscosity reduced to a feasible point, it was transferred to an electronically controlled magnetic stirrer where it was uniformly mixed at high rotational speeds for a duration of ∼5 min. Subsequently, the vacuum was pulled from the beaker and the setup was degassed for 5 min. This was done to expel all the air bubbles that formed during the mixing process. For the next step, a high-temperature release film was clamped on two circular steel plates using metal hoops equipped with adjustable screws. The clamped film was sprayed with ionized air to remove any dust particles or residues. One of the plates was placed on a level surface, and four steel shims each of ∼0.6 mm thickness were placed around the circumference. The degassed mixture was poured on the middle of the plate surface and allowed to spread naturally. It was then quickly covered within 3 min by lowering the second plate, and special care was taken to minimize the formation of air bubbles. The shims ensured that the mixture spread out to an even thickness of ∼0.6 mm. For the first stage of the cure, the mixture was left at ambient temperature and humidity for 18 h. The partially cured epoxy was then subjected to a two-stage cure inside a vacuum oven. The first-stage cure lasted for 90 min, and the oven temperature was set to 65 °C. The temperature was ramped up to 130 °C for the 90 min s stage cure. For each class of cured epoxies, 5−6 circular samples of ∼35 mm diameter were cut out on the drill press using a circular diamond drill bit. All the samples were then dried in the vacuum oven in accordance with ASTM D229.[56] One sample of the OS_200 class has been shown in Figure 2.

Table 1. Epoxy/Hardener Mass Ratios and Class Coding

hardener percentage	epoxy/hardener mass ratio	class coding
100% (stoichiometric)	100:15.2	S_100
150%	100:23	OS_150
180%	100:27.4	OS_180
200%	100:30.4	OS_200

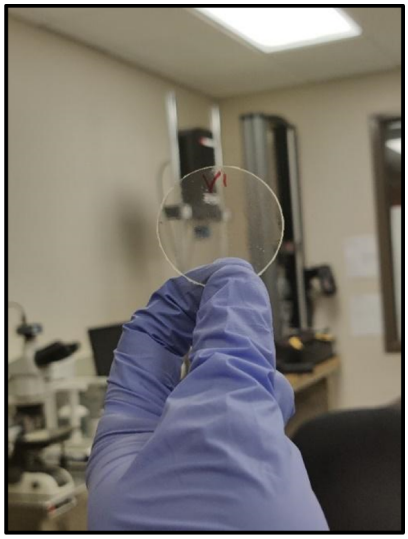

Figure 2. Fully cured over-stoichiometric (OS_200) sample.

2.3. Dynamic Mechanical Analysis. A Discovery DMA 850 by TA Instruments was used for calculating the T_g of each class of cured epoxies. Separate rectangular samples of dimensions 20 × 10 mm were cut using the Buehler IsoMet 1000 Precision Saw for the thermomechanical analysis.

Polymers are viscoelastic materials and exhibit a phase shift (δ) when their oscillating stress and strain behavior are compared. The complex elastic modulus (E^*) of a polymer is given by

$$E^* = E' + iE'' \quad \text{(i)}$$

where E' is the storage modulus which is associated with the stored energy during deformation and E'' is the loss modulus which is associated with the loss in energy during relaxation.[57] The phase angle between E' and E'' is the phase shift δ which can also be represented as

$$\tan\delta = \frac{E''}{E'} \quad \text{(ii)}$$

a DMA scan of any polymer sample is a representation of its mechanical response (change in storage modulus E') under an oscillating strain at varying temperatures. In the case of amorphous

https://doi.org/10.1021/acsapm.2c01570
ACS Appl. Polym. Mater. 2023, 5, 400−411

polymers such as epoxies, the largest drop in E' is triggered at the glass transition (T_g) temperature (α transition). Therefore, the peak position in the tan δ *versus* temperature curve gives a measure of the T_g of the polymer.

For calculating the T_g of the cured epoxies, the tensile clamps were used in the DMA and an oscillating tensile strain of 1 Hz was applied. The temperature was ramped at a rate of 3 °C/min from room temperature (25 °C) to 300 °C.

2.4. Gravimetric Moisture Uptake and Humidity Cycling. The initial experimental outline was to allow the samples to absorb moisture from the ambient conditions in the lab where the thermostat was set at 72 °F and the relative humidity fluctuated between 40 and 60% RH. However, it was observed that besides their network architectures, the moisture uptake profile for all classes of samples was also very sensitive to the humidity in the lab. A transition to more humid weather led to rapid moisture uptake and the absorption slowed down during drier weather patches. We attempted to leverage this phenomenon and analyze the behavior of the samples when they were subjected to cycles of high and low humidity. One cycle was constituted of a 2 week window where the samples were kept in a humidity chamber maintained at 22.5 °C and a 95−99% relative humidity followed by a 2−3 week duration in the ambient lab conditions. The weight of the samples was monitored weekly using the high-precision Mettler-Toledo analytical balance, and the moisture uptake was calculated through the weight change of each sample according to

$$M(\%) = \frac{W - W_i}{W_i} \times 100\% \quad \text{(iii)}$$

where W is the weight of the specimen after absorption for a specific time and W_i is the initial dry weight of the specimen after drying in a vacuum oven. There were five representative samples for each class of cured epoxies, and the moisture uptake level was determined by taking the average of all samples belonging to a particular class.

2.5. Measuring Dielectric Properties. The dielectric properties of the samples were recorded at a microwave frequency of 5 GHz using a SPDR, shown in Figure S1 of the Supporting Information, manufactured by QWED, Poland.[58] In line with our previous studies,[8,37,38,59,60] the SPDR was coupled with an Agilent programmable Vector Network Analyzer (VNA) through high-precision coaxial cables. This setup is capable of measuring bulk relative permittivity, and it can also track minute changes in permittivity (in the order of 10^{-3}). After device calibration, the VNA is used to record the resonant frequency and quality factor (Q-factor) of the empty resonator. The introduction of the sample shifts the resonant frequency of the SPDR, and the relative permittivity can be calculated from the difference in frequencies according to

$$\varepsilon_r' = 1 + \frac{f_0 - f_s}{h f_0 K_\varepsilon(\varepsilon_r', h)} \quad \text{(iv)}$$

where f_0 is the empty resonator frequency, f_s is the SPDR frequency after the sample has been inserted, h is the sample thickness, and K_ε is a function of both ε_r' and h, the values of which are unique to each SPDR and provided in a tabular form by the manufacturer.

For every sample, an average of three measurements was considered as the observed dielectric constant at a particular moisture concentration. In line with Section 2.4, the average dielectric constant of a particular epoxy class was an average of all the samples belonging to that class.

2.6. Infrared Spectroscopy. The Shimadzu UV-3600 spectrophotometer unit was used to obtain the spectral scans of the epoxy samples in the near-infrared (NIR) region. The measurement capabilities of the instrument are flexible and allow sample characterization in the ultraviolet (UV), visible light, and NIR region of up to 3300 nm. The scan range in this study was in the wavelength range of 1250−2500 nm (8000−4000 cm^{-1}) in steps of 1 nm. The unit uses two detector units in the NIR range: an indium/gallium arsenide (InGaAs) photodiode detector which switches to a cooled PbS photoconductive detector at a predefined set point between 1600 and 1800 nm.

The recommended slit width of 5 nm was selected for the light entrance, and the gain on both detectors was set to 3. As a first step, a reference scan was performed without any sample in the holder. One such scan has been included in Figure S2 of the Supporting Information. The absorbance hovers around the expected value of zero, but there are slight variations, especially at lower wavelengths (higher wavenumber). To ensure a uniform zero absorbance in the absence of a sample, the reference was later used for correcting the sample scans. Subsequently, the absorption spectra were collected for all five samples for every epoxy class and an average spectrum at a particular moisture concentration was calculated for further analysis.

3. RESULTS AND DISCUSSION

3.1. Curing Validation through Thermomechanical Analysis. Before analyzing the effects of moisture contamination or the relative concentration of different water species, it was crucial to validate whether the experimental protocol described in Section 2.2 was successful in curing distinct classes of epoxy with varying crosslinking densities. A significant amount of research has been done analyzing the correlation between crosslink density and glass transition temperature (T_g). Both simulation[61] and experimental studies[54,62] have found that increasing the crosslinking density restricts the molecular mobility of the network chains and reduces the viscoelastic behavior of the polymer. As a result, the glassy−rubbery transition happens at a higher temperature and the T_g of the polymer network increases with the degree of crosslinking. As described in Section 2.3, the T_g of the four classes of cured epoxies was obtained from the tan δ *versus* temperature curve and the results have been compiled in Figure 3. Two trends are evident as the hardener concentration

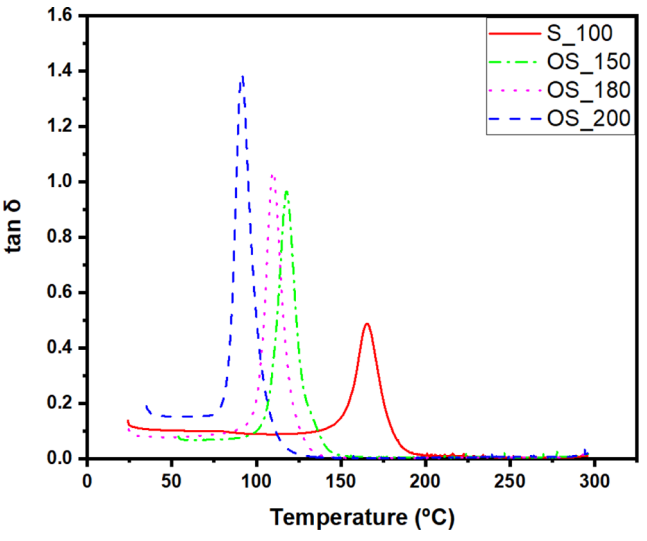

Figure 3. Tan δ *vs* temperature curves for the four classes of cured epoxies.

is increased in the epoxy-the peak positions shift to lower temperatures and the individual peak heights increase. The peak positions signify the α transition (T_g) and the shift to lower temperatures is a clear indication that the degree of crosslinking decreases when over-stoichiometric ratios of hardener are used. The increase in peak heights is evidence of enhanced mobility at greater hardener concentrations. For over-stoichiometric mixtures, a fraction of the DETA

https://doi.org/10.1021/acsapm.2c01570
ACS Appl. Polym. Mater. 2023, 5, 400−411

molecules will be incompletely saturated, generating a lot of flexible free chain ends. In case of extreme excess, there might be completely unreacted DETA molecules which would act as plasticizers in the polymer and further reduce the T_g. The segmental motion of the short-chain segments will increase the viscoelastic behavior of the polymer network as a greater percentage of the applied mechanical load would be dissipated. This will lead to a higher loss modulus (E'') and as observed in eq (ii), the magnitude of tan δ will increase as a consequence. The results in Figure 3 vindicate the curing protocol and validates the sequential decrease in crosslinking in the different sample classes. The storage modulus (E') can also provide additional information about the curing progression in the epoxies as its value in the rubbery plateau region is correlated with the number of crosslinks in the polymer chain. The molecular weight between crosslinks (M_w) for all the epoxy batches has been calculated in Section S3 of the Supporting Information. The results in Figure S3 clearly indicate that M_w increases sequentially as the curing mixtures become increasingly over-stoichiometric. Therefore, as the average molecular weight of the oligomers between two junctions decreases, the network becomes densely crosslinked and exhibits a higher glass transition temperature (T_g).

3.2. Moisture Uptake Profile. Section 2.4 alludes to the phenomenon initially observed in these samples with respect to moisture absorption as the humidity changed inside the lab. Figure 4 presents the gravimetric moisture uptake in the cured

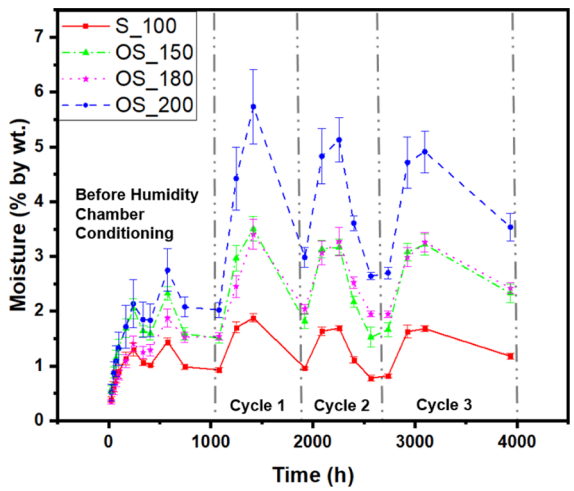

Figure 4. Moisture absorption profile of the cured epoxies subjected to cycles of fluctuating humidity.

epoxies as a function of time. Every recorded observation in the figure is an average moisture concentration of a particular class of cured epoxy, and the error bars in the figure signify the standard deviation across the five samples of a particular class. The initial experimental plan was to study the absorption trends in these cured epoxies and analyze the corresponding changes in their dielectric properties and spectral profiles. In accordance with this outline, all the samples were kept in the ambient lab environment and during the initial uptake duration of ~250 h, and a linear absorption profile was observed in all the samples. However, fluctuations in lab humidity due to weather changes led to a uniform rise and fall in moisture concentrations for all the sample classes between ~250 and 1000 h. It was also seen that the changes induced by humidity were more pronounced in over-stoichiometric sample classes. After observing this behavior, we concluded that in addition to studying the inherent morphological differences in these sample classes, it will be interesting to incorporate the effects of fluctuating cycles of humidity on the polymer networks. Therefore, as described in Section 2.4, the samples were periodically introduced in the high-humidity chamber and taken back into the ambient lab conditions. As illustrated by the black dotted lines in Figure 4, a total of three such cycles were completed. The higher degree of absorption inside the humidity chamber was expected, but the cyclic trends in the figure demonstrate how the departure from the stoichiometric curing ratio leads to a sequential rise in moisture concentration at the same temporal point. For the same time duration in the chamber, the OS_200 samples absorbed significantly more moisture when compared to the S_100 samples. Additionally, after the samples were brought out of the chamber in any cycle, desorption allowed the S_100 samples to consistently return to a moisture content which was close to the preconditioned levels seen before the cycling. On the other hand, the over-stoichiometric samples never completely returned to the precycling state. Samples from all the epoxy classes retained a certain degree of residual moisture at the end of the third humidity cycle, the fraction of which was the highest for the OS_200 samples. These results consolidate the hypothesis that a combination of higher polarity and additional free volume generated in the more flexible over-stoichiometric networks allow them to absorb and retain more moisture after being subjected to a cycle of high and low humidity.

3.3. Dielectric Properties. In Section 3.2, we discussed how the differences in curing chemistry can significantly alter the moisture absorption profile, which in theory should have concurrent effects on the dielectric properties. The average change in the dielectric constant compared to the dry baseline of each sample class was recorded over time, and the results have been visually communicated in Figure 5a. As expected, the trends in Figure 5a bear a close correlation with the ones seen in Figure 4.

Despite similar chemical constituents, the epoxies with a higher concentration of hardener exhibit a much higher change in relative permittivity, which is primarily driven by the enhanced degree of moisture absorption in these samples. The OS_200 samples which consistently absorb more moisture during the humidity cycles also have the highest changes in permittivity, and the residual moisture in the over-stoichiometric mixtures has a permanent impact on their dielectric properties as the relative permittivity of these samples never returns to their preconditioned state. The high degree of linear correlation between the dielectric properties and the corresponding moisture concentration in the cured epoxies is also evidenced in the magnitudes of R^2 compiled in Figure 5b.

3.4. Analyzing the NIR Spectra. *3.4.1. Quantifying the Absorption Peak Areas.* The average NIR spectra for an S_100 epoxy after 408 h of ambient exposure (1.02% moisture by wt) are shown in Figure 6a. These scans obtained from the spectrophotometer require some form of baseline correction prior to quantitative analysis. The correction is done by subtracting a linear or polynomial fit which can remove the tilted variations across the wavenumber scale.[63] In this study, Origin 2018b was used to subtract a linear baseline similar to the one included in Figure S4 from all the scans to yield corrected scans compiled in Figure 6b. The spectra are for the S_100 samples at different moisture concentrations corresponding to ambient exposure times. We can see in the figure

https://doi.org/10.1021/acsapm.2c01570
ACS Appl. Polym. Mater. 2023, 5, 400−411

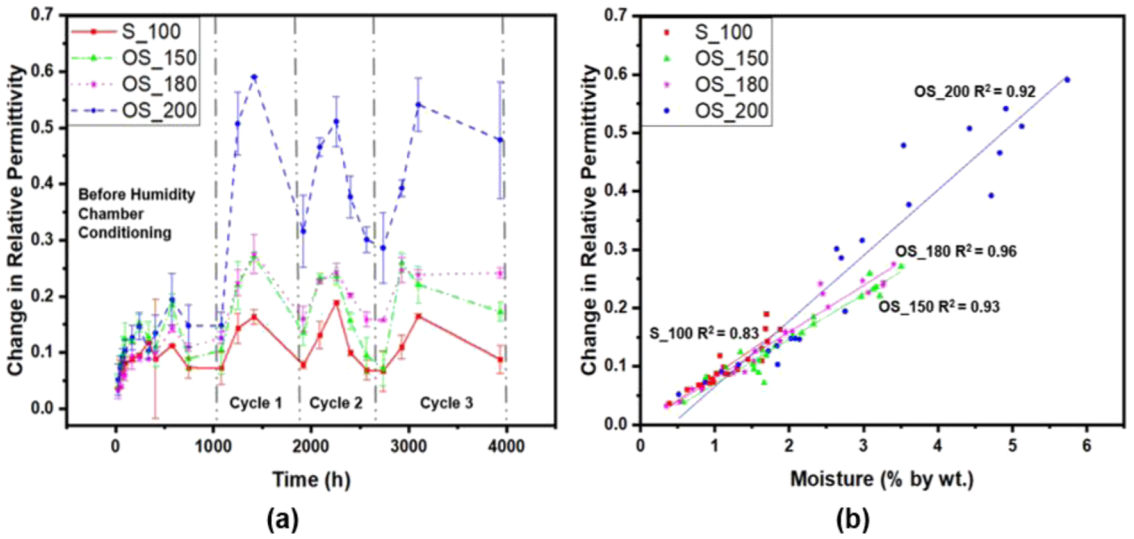

Figure 5. (a) Change in relative permittivity of the cured samples subjected to cycles of fluctuating humidity. (b) Linear correlation between moisture concentration and changes in relative permittivity.

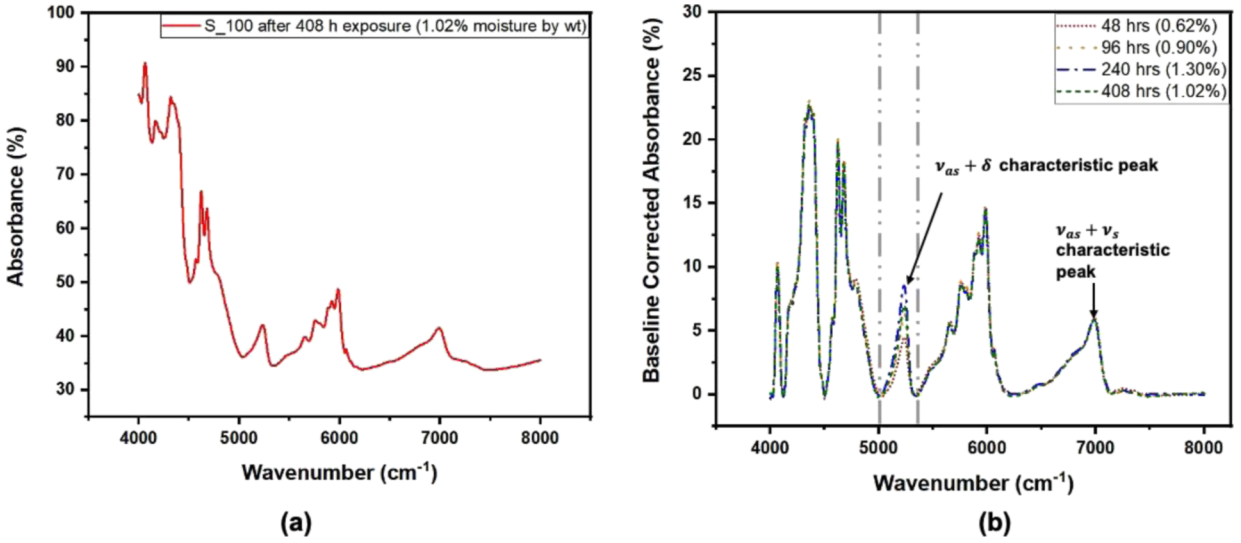

Figure 6. (a) S_100 NIR spectra after 408 h of exposure (1.02% moisture by wt). (b) Corrected NIR spectra for the S_100 epoxies after different durations of ambient exposure. Values in parenthesis indicate moisture concentration by wt at the observation points.

that the scans practically superimpose on each other except for the contributions of absorbed water which is manifested in the characteristic peak at ~5215 cm^{-1}. Previous studies[23,64] have identified this peak to be a combination of the asymmetric stretching (ν_{as}) and the in-plane deformation (δ) of water occurring, respectively, at 3755 and 1595 cm^{-1}. In case of a crosslinked epoxy, this peak is well resolved and is free from interference by any other functional groups in the polymer network. There is another characteristic water peak ~6900 cm^{-1} which is due to the combination of the asymmetric and symmetric stretching (ν_{as} and ν_s) of the hydroxyl (OH) bond in the water molecules.[24] However, this absorption band includes the strong effects superimposed by the first OH overtone of the hydroxyl groups in the epoxy resin, making it harder to resolve for analysis.[65] Figure 6b shows clear signs that the area of the peak centered at 5215 cm^{-1} is correlated with the moisture content, and it was used for quantifying the moisture concentration in the samples. To isolate the effects of water, the dry spectra of the cured epoxies were subtracted at different moisture concentrations and only the absorption band between 5000 and 5230 cm^{-1} was considered. Figure 7a illustrates the water peak areas of each sample class as they are subjected to moisture exposure over time. The trends corroborate the ones observed during the moisture uptake and the subsequent changes in relative permittivity. The high degree of linear correlation between the peak area and permittivity changes, evidenced by the R^2 values in Figure 7b, also validates the hypothesis that moisture absorption is the primary contributor driving the relative permittivity changes in these samples. In terms of practical implications, the results in this section indicate that the peak area can be used to develop a predictive model which can quantify the moisture concentration in epoxy samples if the curing chemistry is known.

3.4.2. Relative Concentration of the Different Water Species. The combination band ($\nu_{as} + \delta$) at ~5215 cm^{-1} has been previously analyzed at different temperatures.[64] Buijs and Choppin[66] were successful in decomposing this peak into three

https://doi.org/10.1021/acsapm.2c01570
ACS Appl. Polym. Mater. 2023, 5, 400−411

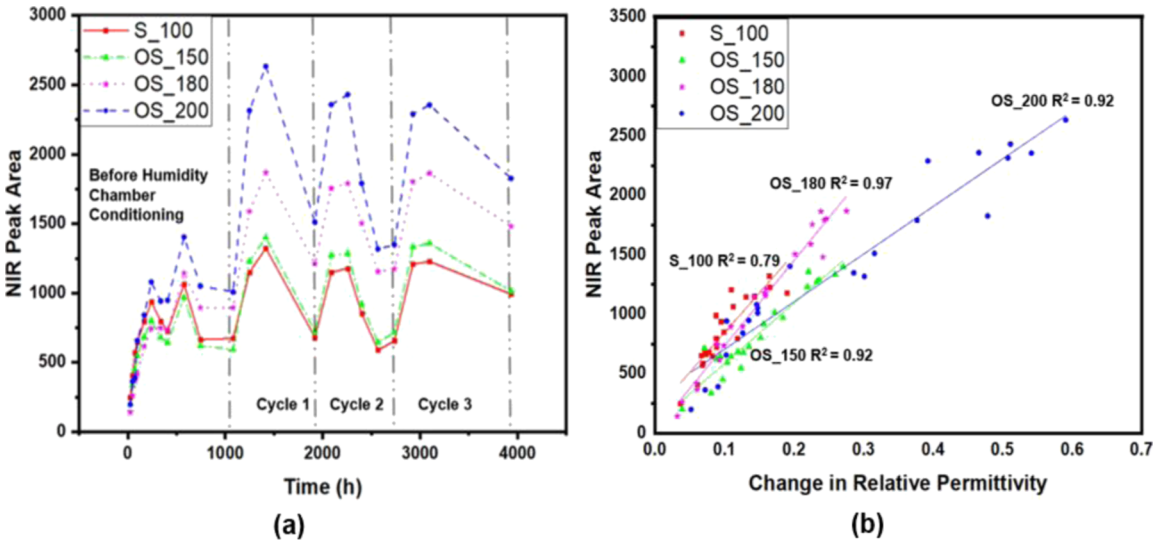

Figure 7. (a) Change in the spectral water peak area of the cured samples subjected to cycles of fluctuating humidity. (b) Linear correlation between changes in relative permittivity and the NIR peak area.

component bands and postulated that bulk water is composed of three distinct species. The lowest frequency band is attributed to the S_2 water molecules which are tightly bound and engaged in multiple hydrogen bonds (HBs).[64] The loosely bound water molecules with one active HB contribute to the S_1 band, while the highest frequency band (S_0) near the 5230 cm^{-1} wavenumber is constituted of free water molecules which are neither HB donors nor acceptors.[66] In this work, the absorbance spectra of the water peak were resolved into these individual bands by fitting a mixed Gaussian−Lorentzian function.[24] PeakFit v4.12 software was used for the deconvolution which allows choosing the desired number of resolvable peaks and their approximate centers.[67] It then locally varies the center and the full width at half-maximum (fwhm) of these peaks to minimize the sum of squared error between the composite fitted peak and the original spectra. The fits were iteratively improved until the coefficient of determination (R^2) reached a minimum value of 0.99. For a particular moisture concentration (~2% moisture by wt) of each epoxy class, the model fit formed by the three deconvoluted peaks has been overlaid on the recorded NIR spectra and shown in Figure S5a−d. The area occupied by the resolved Gaussian−Lorentzian peaks (A_x) can be subsequently used to calculate the relative distribution of the S_0, S_1, and S_2 water species. Consistent with previous studies,[24,25] the S_0 (no HB) and S_1 (1 active HB) water molecules were considered equivalent in terms of molar absorptivity ($a_{S_0} \cong a_{S_1}$) and denoted as free water, while the S_2 water molecules were considered bound. The ratio between the bound and free water molar absorptivity $\left(\frac{a_{S_0}}{a_{S_2}}\right)$ has been previously calculated to be ~0.81.[24] Relative free (C_{free}) and bound (C_{bound}) water concentrations can then be determined by using the relationship

$$\frac{C_{free}}{C_{tot}} = \frac{A_{S_0} + A_{S_1}}{A_{S_0} + A_{S_1} + \frac{a_{S_0}}{a_{S_2}} A_{S_2}} \quad \text{(va)}$$

$$\frac{C_{bound}}{C_{tot}} = 1 - \frac{C_{free}}{C_{tot}} \quad \text{(vb)}$$

The variation in these concentrations as a function of moisture content for the stoichiometric (S_100) and over-stoichiometric, OS_200, epoxies has been plotted in Figure 8.

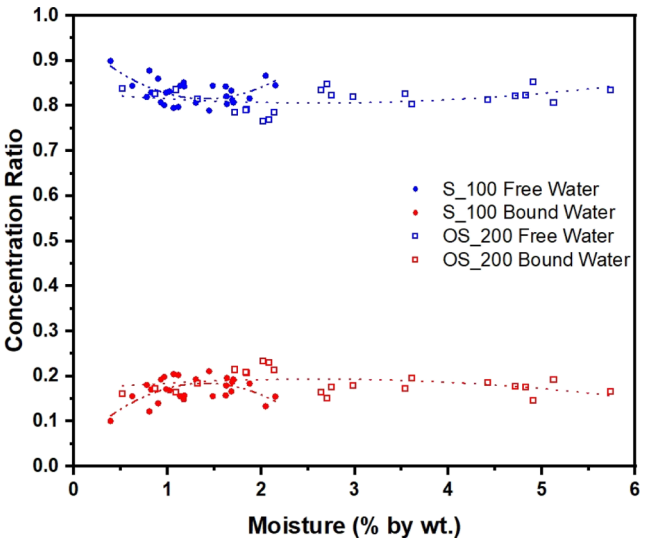

Figure 8. Variation of free and bound water concentrations as a function of moisture content in the S_100 and OS_200 epoxies.

The trends for OS_150 and OS_180 were very similar to those for OS_200 and have been included in Figure S6 of the Supporting Information. We can observe that the free-to-bound water ratio in both classes varies approximately between 90:10 and 80:20 across moisture concentrations. It has been previously reported that ~90% of absorbed moisture in polymers is in the free state[68] which matches our findings in the stoichiometric mixture (S_100). In the case of these samples, we observe a nonlinear variation in the ratio as the moisture concentration increases. At lower moisture concentrations, the ratio is higher (~90:10), but as moisture is absorbed into the system, a higher fraction of water molecules engage in strong HBs with the polar sites in the network and increase the bound water contributions. A slight rise in the ratio at higher moisture concentrations can be attributed to the

https://doi.org/10.1021/acsapm.2c01570
ACS Appl. Polym. Mater. 2023, 5, 400−411

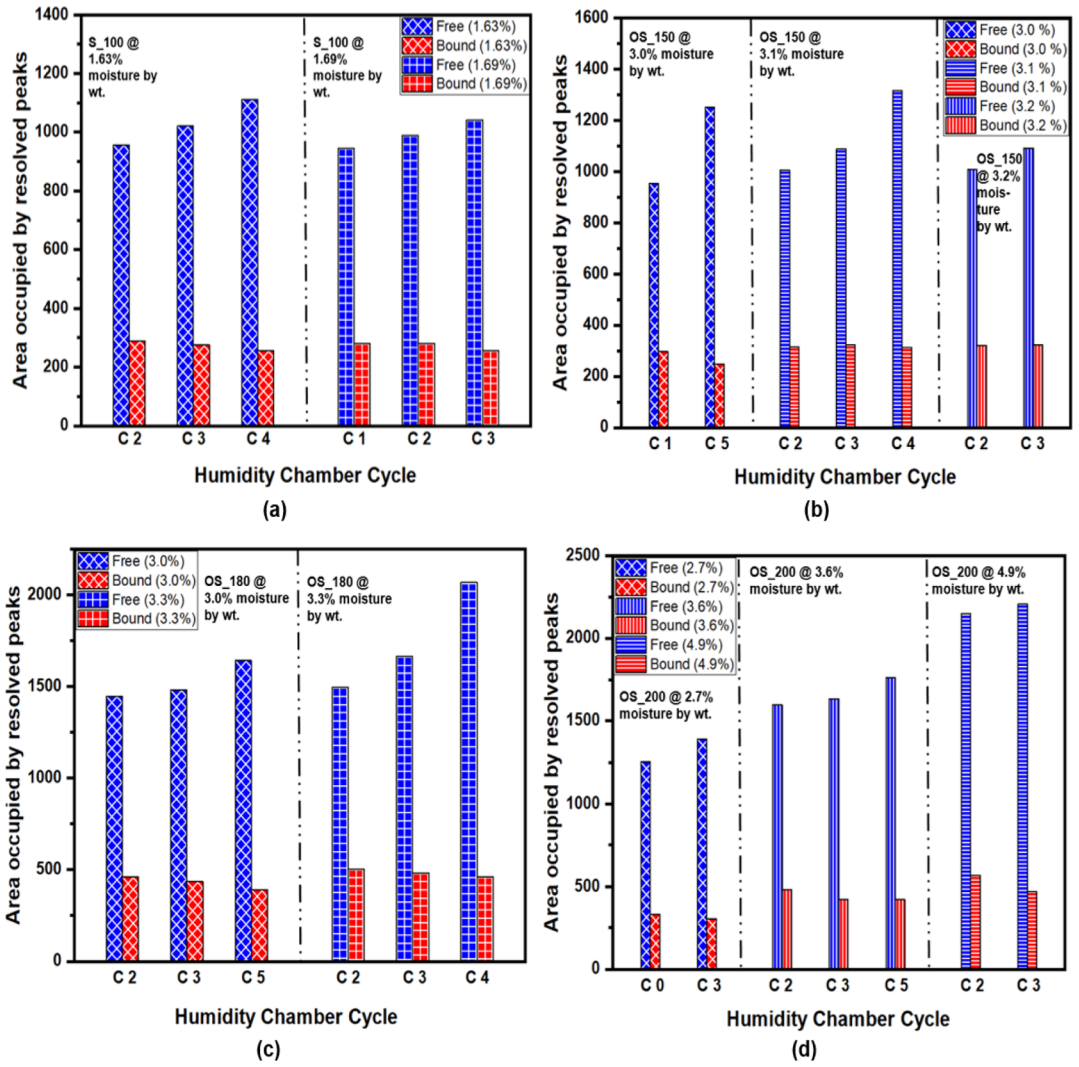

Figure 9. Area occupied by the resolved free and bound water peaks at the same moisture concentrations at subsequent cycles of high humidity for (a) S_100, (b) OS_150, (c) OS_180, and (d) OS_200 epoxies. Cycles have been denoted with the letter "C" in the figure.

additional free volume generated by the moisture-induced swelling in the network. Studies have postulated that water bound to the polar sites contributes to the swelling, but as these molecules slide between polymer chains, they increase the available free volume in the network.[20] Since intermolecular secondary bonding begins with the initiation of absorption, long-term exposure can generate enough free volume for some redistribution between the free and bound water ratios at higher moisture concentrations. We reported a similar phenomenon in our previous work[29] where the free-to-bound ratio slightly increased from the higher available free volume created at greater degrees of crosslinking. In case of the over-stoichiometric epoxies, a much flatter trend is observed as the samples absorb moisture. There was a higher population of polar sites in these samples which increased the bound water concentrations across moisture concentrations. The free volume for these classes of epoxies was inherently greater due to the flexible polymer chains which contributed to the broadly uniform free-to-bound ratios throughout the exposure and humidity cycling regime.

3.4.3. Consequences of Humidity Cycling. A closer look at Figure 4 reveals that during the cycles of absorption and desorption, the samples coincidentally reached very similar moisture concentrations. For instance, the S_100 samples had a moisture concentration of 1.63317 and 1.62719% by wt at 2088 and 2927 h of exposure, respectively. These values can be reasonably approximated as an average moisture content of 1.63%. Similar sets of repeating observations were found in the other classes of epoxies. However, as seen in Figure S7a, when the characteristic water peak of these NIR scans for the S_100 sample is plotted, the peak height is greater when the sample reaches 1.63% moisture in the third humidity cycle (2927 h). Another important conclusion can be drawn from Figure S7a–d where we observe that the entire peak does not shift to higher absorbance values. At both lower (<5125 cm^{-1}) and higher wavenumbers (>5300 cm^{-1}), there are minimal reductions in the peak area. It is important to acknowledge here that even in the absence of humidity fluctuations, the NIR peaks at similar moisture concentrations for the same epoxy sample will not be exactly reproduced. The moisture concentrations are an average value across five samples, and as mentioned above, there are slight differences in these values in subsequent cycles. The NIR peak being studied is also an average spectrum of the five samples. There are some other sources of approximations like the subtraction of the reference spectra (Figure S2, Section 2.4) and minor errors introduced

https://doi.org/10.1021/acsapm.2c01570
ACS Appl. Polym. Mater. 2023, 5, 400−411

by baseline corrections (Figure S4, Section 3.4.1). Despite these limitations, the qualitative trends in the bound and free water peak areas at a similar moisture content can serve as an indicator of morphological changes induced in the networks by preceding absorption cycles. To test this hypothesis across a wider data set, all the samples which were kept in the ambient lab environment after the third humidity cycle were subjected to two additional cycles of absorption and desorption, and the results of the uptake were appended together with the previous three humidity cycles as shown in Figure S8. The uptake plots indicate that during the prolonged exposure to the ambient lab conditions, the samples absorbed a small degree of moisture. Following the previous trends, the ambient absorption was lowest in the S_100 epoxies, while the OS_200 samples absorbed the most amount of moisture. The uptake behavior in the last two high-humidity cycles was similar in nature to the previous three, but the peak moisture concentrations were notably higher, especially for the over-stoichiometric epoxy samples. This is consistent with our hypothesis that absorbed moisture alters the network morphology and induces a higher concentration of free volume. Analyzing the data in Figure S8 revealed that in each epoxy class, there were at least two distinct moisture concentrations which were reached by the samples in multiple humidity cycles. Consequently, the area occupied by the resolved free and bound water peaks at these unique moisture uptakes is plotted in Figure 9a−d. The *x*-axis in the figure denotes the humidity cycle at which the moisture concentration was observed, and black dotted lines have been used in the subplots to distinguish between distinct moisture levels in the same epoxy class. In case a particular moisture concentration was observed before the first cycle in the humidity chamber, then that reading has been denoted as cycle 0 (Figure 9d). The hypothesis which was formulated after observing the shift in peak height in Figure S7a−d is validated by the trends observed in each subplot of Figure 9. Absorption of moisture creates additional free volume in each of the polymer networks which is preserved even after desorption. When the same level of moisture uptake is reached in subsequent cycles, the greater free volume enables a higher fraction of water molecules to be in the loosely bound (S_1) or completely unbound (S_0) states which manifests in a greater resolved peak area for free water. On the other hand, the bound water area which is dictated by the intermolecular hydrogen bonding decreases with a weak trend as more water molecules exist in the S_0 (free) or S_1 (loosely bound) form. The results from this section demonstrate that subjecting an epoxy matrix through periodic cycles of fluctuating humidity can trigger degradation mechanisms which will lead to a higher fraction of free water even at the same moisture content. Since the relative concentration of free water significantly influences matrix swelling, plasticization, and overall mechanical properties,[69] epoxy resins used as composite matrices will degrade in service even in the absence of any externally induced damage.

4. CONCLUSIONS

In order to experimentally validate the inferences drawn from previous molecular scale studies, separate batches of epoxies with different network morphologies were fabricated. The variation in crosslinking density for the different sample classes was supported and confirmed by the results of DMA. The effects of network architecture were reflected in the gravimetric moisture uptake results. During moisture uptake, subtle changes in ambient humidity were observed to impact the moisture concentration, prompting additional scrutiny of the effects of fluctuating humidity cycles on the absorption process. The results showed that cured epoxies with the lowest crosslinking density and highest polarity exhibited a maximum moisture concentration, which was approximately 3.3 times higher than the stoichiometric samples with the highest crosslinking density. The dielectric properties and characteristic moisture peak absorbance area obtained from the SPDR and NIR spectrophotometer, respectively, closely tracked the trends in moisture absorption—supporting the hypothesis that the extent of moisture contamination is directly correlated with the dielectric properties of the epoxies. During the postprocessing of the NIR results, it was observed that when samples of any class reached very similar average moisture concentrations after subsequent desorption−absorption cycles, the characteristic peak heights shifted to higher values. To further investigate this phenomenon, equivalent moisture concentrations were identified in all epoxy classes. The area occupied by the resolved free and bound water peaks was plotted with the corresponding humidity chamber cycle when the observation was recorded. The sequential rise around the free water peaks with increasing high-humidity cycles suggests that moisture-induced swelling creates additional free volume sites during absorption, which are subsequently retained in the polymer network even after desorption. Consequently, when the same moisture absorption is achieved, the two species of water molecules are redistributed in a manner that enables a higher fraction of free water. The results from this study reinforce the importance of periodic health monitoring of polymer-based structural materials to assess in-service degradation from matrix plasticization and absorption-induced damage, even in the absence of mechanical damage. It also highlights the need for future investigations involving a nano-NIR setup which can spatially quantify the free-to-bound water ratio in a moisture-contaminated polymer matrix sample and detect localized areas with the highest concentrations of absorption-induced microcracks, nanopores, and voids.

■ ASSOCIATED CONTENT

Supporting Information

The Supporting Information is available free of charge at https://pubs.acs.org/doi/10.1021/acsapm.2c01570.

SPDR image, reference scan in NIR without the sample, average molecular weight between crosslinks, linear baseline subtraction, deconvoluted peaks for the different water species, relative concentrations of water species in the cured epoxy classes, NIR absorbance peaks at similar moisture concentrations in different humidity cycles, and additional high humidity cycles (PDF)

■ AUTHOR INFORMATION

Corresponding Author

Landon R. Grace − *Department of Mechanical and Aerospace Engineering, North Carolina State University, Raleigh, North Carolina 27606, United States;* orcid.org/0000-0001-6358-745X; Phone: +1-(405)-306-6474; Email: lgrace2@ncsu.edu

https://doi.org/10.1021/acsapm.2c01570
ACS Appl. Polym. Mater. 2023, 5, 400−411

Authors

Rishabh D. Guha − *Department of Mechanical and Aerospace Engineering, North Carolina State University, Raleigh, North Carolina 27606, United States*

Evgeny O. Danilov − *Department of Chemistry, North Carolina State University, Raleigh, North Carolina 27695, United States;* orcid.org/0000-0002-5551-3749

Katherine Berkowitz − *Department of Mechanical and Aerospace Engineering, North Carolina State University, Raleigh, North Carolina 27606, United States*

Oluwatimilehin Oluwajire − *Department of Mechanical and Aerospace Engineering, North Carolina State University, Raleigh, North Carolina 27606, United States*

Complete contact information is available at: https://pubs.acs.org/10.1021/acsapm.2c01570

Funding

This material is based upon work partially supported by the National Science Foundation under grant no. CMMI-175482.

Notes

The authors declare no competing financial interest.

■ ACKNOWLEDGMENTS

The authors gratefully acknowledge Dr. Ogheneovo Idolor for helpful discussions on the epoxy curing procedure, Dr. Salma Siddika (NCSU) for her assistance with the DMA experiments, and Dr. Felix Castellano for allowing them to use the NIR setup at the Imaging and Kinetic Spectroscopy Laboratory (IMAKS) at the Department of Chemistry, NCSU.

■ REFERENCES

(1) Reports and Data Composites Market To Reach USD 146.14 Billion By 2026. https://www.globenewswire.com/news-release/2019/04/09/1799898/0/en/Composites-Market-To-Reach-USD-146-14-Billion-By-2026-Reports-And-Data.html (accessed April 09, 2019).

(2) Ellyin, F.; Rohrbacher, C. The Influence of Aqueous Environment, Temperature and Cyclic Loading on Glass-Fibre/Epoxy Composite Laminates. *J. Reinf. Plast. Compos.* **2003**, *22*, 615−636.

(3) Debska, B.; Lichołai, L.; Lichołai, L. Resin composites with high chemical resistance for application in civil engineering. *Period. Polytech. Civ. Eng.* **2016**, *60*, 281−287.

(4) Seo, J.; Jang, W.; Han, H. Thermal properties and water sorption behaviors of epoxy and bismaleimide composites. *Macromol. Res.* **2007**, *15*, 10−16.

(5) Grace, L. R. The effect of moisture contamination on the relative permittivity of polymeric composite radar-protecting structures at X-band. *Compos. Struct.* **2015**, *128*, 305−312.

(6) Daniel, I. M.; Ishai, O.; Daniel, I. M.; Daniel, I.*Engineering Mechanics of Composite Materials*; Oxford University Press: New York, 2006.

(7) Fiore, V.; Valenza, A.Epoxy resins as a matrix material in advanced fiber-reinforced polymer (FRP) composites. *Advanced Fibre-Reinforced Polymer (FRP) Composites for Structural Applications*; Elsevier, 2013; pp 88−121.

(8) Idolor, O.; Guha, R.; Grace, L.A Dielectric Resonant Cavity Method for Monitoring of Damage Progression in Moisture-Contaminated Composites*Proceedings of the American Society for Composites—Thirty-Third Technical Conference*; Technomic Publishing Company, 2018.

(9) Soles, C. L.; Yee, A. F. A discussion of the molecular mechanisms of moisture transport in epoxy resins. *J. Polym. Sci., Part B: Polym. Phys.* **2000**, *38*, 792−802.

(10) Zafar, A.; Bertocco, F.; Schjødt-Thomsen, J.; Rauhe, J. C. Investigation of the long term effects of moisture on carbon fibre and epoxy matrix composites. *Compos. Sci. Technol.* **2012**, *72*, 656−666.

(11) Grace, L. R.; Altan, M. C. Characterization of anisotropic moisture absorption in polymeric composites using hindered diffusion model. *Composites, Part A* **2012**, *43*, 1187−1196.

(12) Grace, L. R.; Altan, M. C. Non-fickian three-dimensional hindered moisture absorption in polymeric composites: Model development and validation. *Polym. Compos.* **2013**, *34*, 1144−1157.

(13) Enns, J. B.; Gillham, J. K. Effect of the Extent of Cure on the Modulus, Glass Transition, Water Absorption, and Density of an Amine-Cured Epoxy. *J. Appl. Polym. Sci.* **1983**, *28*, 2831.

(14) Berkowitz, K.; Guha, R. D.; Oluwajire, O.; Grace, L.A Machine Learning Approach for Impact Damage Quantification in Polymer Matrix Composites. *Proceedings of the American Society for Composites-Thirty-Seventh Technical Conference*; DEStech Publications, Inc., 2022.

(15) Bhuyan, M. K.; Bhuyan, M. S.; Rodríguez-Dévora, J. I.; Yanez, M. Delamination behavior of bidirectional S2 glass epoxy laminated composite due to combined moisture and temperature cyclic loading. *J. Compos. Mater.* **2013**, *47*, 3421−3432.

(16) Wong, E. H. Characterizing the kinetics of free and bound water using a non-isothermal sorption technique. *Dry. Technol.* **2017**, *35*, 46−54.

(17) Grace, L. R.; Altan, M. C. Three-dimensional anisotropic moisture absorption in quartz-reinforced bismaleimide laminates. *Polym. Eng. Sci.* **2014**, *54*, 137−146.

(18) Popineau, S.; Rondeau-Mouro, C.; Sulpice-Gaillet, C.; Shanahan, M. E. Free/bound water absorption in an epoxy adhesive. *Polymer* **2005**, *46*, 10733−10740.

(19) Garden, L.; Pethrick, R. A. A dielectric study of water uptake in epoxy resin systems. *J. Appl. Polym. Sci.* **2017**, *134*, 44717.

(20) Adamson, M. J. Thermal expansion and swelling of cured epoxy resin used in graphite/epoxy composite materials. *J. Mater. Sci.* **1980**, *15*, 1736−1745.

(21) Mijović, J.; Zhang, H. Local Dynamics and Molecular Origin of Polymer Network−Water Interactions as Studied by Broadband Dielectric Relaxation Spectroscopy, FTIR, and Molecular Simulations. *Macromolecules* **2003**, *36*, 1279−1288.

(22) Herrera-Gómez, A.; Velázquez-Cruz, G.; Martín-Polo, M. O. Analysis of the water bound to a polymer matrix by infrared spectroscopy. *J. Appl. Phys.* **2001**, *89*, 5431−5437.

(23) Musto, P.; Ragosta, G.; Scarinzi, G.; Mascia, L. Probing the molecular interactions in the diffusion of water through epoxy and epoxy-bismaleimide networks. *J. Polym. Sci., Part B: Polym. Phys.* **2002**, *40*, 922−938.

(24) Musto, P.; Ragosta, G.; Mascia, L. Vibrational Spectroscopy Evidence for the Dual Nature of Water Sorbed into Epoxy Resins. *Chem. Mater.* **2000**, *12*, 1331−1341.

(25) Idolor, O.; Guha, R. D.; Berkowitz, K.; Geiger, C.; Davenport, M.; Grace, L. Polymer-water interactions and damage detection in polymer matrix composites. *Composites, Part B* **2021**, *211*, 108637.

(26) Idolor, O.; Guha, R. D.; Berkowitz, K.; Grace, L. R.Damage Detection in Polymer Matrix Composites by Analysis of Polymer-Water Interactions using Near-Infrared Spectroscopy. *Proceedings of the American Society for Composites—Thirty-Fifth Technical Conference*; Technomic Publishing Company, 2020.

(27) Oluwajire, O.; Berkowitz, K.; Guha, R. D.; Grace, L.Experimental Validation of the Dynamic Molecular State of Water in Damaged Polymer Composites Using Near Infrared Spectroscopy. *Proceedings of the American Society for Composites-Thirty-Seventh Technical Conference*; DEStech Publications, Inc., 2022.

(28) Mijović, J.; Zhang, H. Molecular Dynamics Simulation Study of Motions and Interactions of Water in a Polymer Network. *J. Phys. Chem. B* **2004**, *108*, 2557−2563.

(29) Guha, R. D.; Idolor, O.; Grace, L. An atomistic simulation study investigating the effect of varying network structure and polarity in a moisture contaminated epoxy network. *Comput. Mater. Sci.* **2020**, *179*, 109683.

(30) Guha, R. D.; Idolor, O.; Berkowitz, K.; Pasquinelli, M.; Grace, L. R. Exploring secondary interactions and the role of temperature in moisture-contaminated polymer networks through molecular simulations. *Soft Matter* **2021**, *17*, 2942−2956.
(31) Guha, R. D.; Rahmani, F.; Berkowitz, K.; Pasquinelli, M.; Grace, L. R. Temporal evolution of the behavior of absorbed moisture in a damaged polymer-quartz composite: A molecular dynamics study. *Comput. Mater. Sci.* **2022**, *214*, 111690.
(32) Guha, R. D.; Idolor, O.; Grace, L.Molecular Dynamics (MD) Simulation of a Polymer Composite Matrix with Varying Degree of Moisture: Investigation of Secondary Bonding Interactions. *Proceedings of the American Society for Composites—Thirty-Fourth Technical Conference*; Technomic Publishing Company, 2019.
(33) Wu, C.; Xu, W. Atomistic simulation study of absorbed water influence on structure and properties of crosslinked epoxy resin. *Polymer* **2007**, *48*, 5440−5448.
(34) Tam, L.; Lau, D.; Wu, C. Understanding interaction and dynamics of water molecules in the epoxy via molecular dynamics simulation. *Mol. Simul.* **2019**, *45*, 120−128.
(35) Pethrick, R. A.; Hollins, E. A.; McEwan, L.; Pollock, A.; Hayward, D.; Johncock, P. Effect of cure temperature on the structure and water absorption of epoxy/amine thermosets. *Polym. Int.* **1996**, *39*, 275−288.
(36) Fernández, D. P.; Mulev, Y.; Goodwin, A.; Sengers, J. L. A database for the static dielectric constant of water and steam. *J. Phys. Chem. Ref. Data* **1995**, *24*, 33−70.
(37) Idolor, O.; Guha, R.; Bilich, L.; Grace, L.2-Dimensional Mapping of Damage in Moisture Contaminated Polymer Composites Using Dielectric Properties. *Proceedings of the American Society for Composites—Thirty-Fourth Technical Conference*; Technomic Publishing Company, 2019.
(38) Idolor, O.; Berkowitz, K.; Guha, R. D.; Grace, L. Non-destructive Examination of Polymer Composites by Analysis of Polymer-Water Interactions and Damage-Dependent Hysteresis. *Compos. Struct.* **2022**, *287*, 115377.
(39) Tran, A. P.; Ardekani, M. R. M.; Lambot, S. Coupling of dielectric mixing models with full-wave ground-penetrating radar signal inversion for sandy-soil-moisture estimation. *Geophysics* **2012**, *77*, H33−H44.
(40) Hallikainen, M. T.; Ulaby, F. T.; Dobson, M. C.; El-rayes, M. A.; Wu, L. Microwave dielectric behavior of wet soil-part 1: Empirical models and experimental observations. *IEEE Trans. Geosci. Rem. Sens.* **1985**, *GE-23*, 25−34.
(41) Crawford, E.; Lesser, A. J. The effect of network architecture on the thermal and mechanical behavior of epoxy resins. *J. Polym. Sci., Part B: Polym. Phys.* **1998**, *36*, 1371−1382.
(42) Lesser, A. J.; Crawford, E. The role of network architecture on the glass transition temperature of epoxy resins. *J. Appl. Polym. Sci.* **1997**, *66*, 387−395.
(43) Soles, C. L.; Chang, F. T.; Gidley, D. W.; Yee, A. F. Contributions of the nanovoid structure to the kinetics of moisture transport in epoxy resins. *J. Polym. Sci., Part B: Polym. Phys.* **2000**, *38*, 776−791.
(44) Soles, C. L.; Chang, F. T.; Bolan, B. A.; Hristov, H. A.; Gidley, D. W.; Yee, A. F. Contributions of the nanovoid structure to the moisture absorption properties of epoxy resins. *J. Polym. Sci., Part B: Polym. Phys.* **1998**, *36*, 3035−3048.
(45) Calventus, Y.; Montserrat, S.; Hutchinson, J. M. Enthalpy relaxation of non-stoichiometric epoxy-amine resins. *Polymer* **2001**, *42*, 7081−7093.
(46) Morgan, R. J.; Kong, F.; Walkup, C. M. Structure-property relations of polyethertriamine-cured bisphenol-A-diglycidyl ether epoxies. *Polymer* **1984**, *25*, 375−386.
(47) Garcia, F. G.; Soares, B. G.; Pita, V. J.; Sánchez, R.; Rieumont, J. Mechanical properties of epoxy networks based on DGEBA and aliphatic amines. *J. Appl. Polym. Sci.* **2007**, *106*, 2047−2055.
(48) De Nograro, F. F.; Guerrero, P.; Corcuera, M. A.; Mondragon, I. Effects of chemical structure of hardener on curing evolution and on the dynamic mechanical behavior of epoxy resins. *J. Appl. Polym. Sci.* **1995**, *56*, 177−192.
(49) Nguyen, V. T.; Vaughan, A. S.; Lewin, P. L.; Krivda, A. The effect of resin stoichiometry and nanoparticle addition on epoxy/silica nanodielectrics. *IEEE Trans. Dielectr. Electr. Insul.* **2015**, *22*, 895−905.
(50) Rajasekaran, R.; Alagar, M. Bismaleimides (1,3-Bismaleimidobenzene and 1,1′-bis(4-Maleimidophenyl) Cyclohexane) Modified Polyethersulfone/Epoxy Matrices for Engineering Applications. *J. Compos. Mater.* **2008**, *42*, 1031−1043.
(51) Possart, G.; Presser, M.; Passlack, S.; Geiß, P. L.; Kopnarski, M.; Brodyanski, A.; Steinmann, P. Micro-macro characterisation of DGEBA-based epoxies as a preliminary to polymer interphase modelling. *Int. J. Adhes. Adhes.* **2009**, *29*, 478−487.
(52) Alhabill, F. N.; Andritsch, T.; Vaughan, A. S.On water absorption and its impact on the dielectric spectra of epoxy network with different stoichiometries. *2017 IEEE Conference on Electrical Insulation and Dielectric Phenomenon (CEIDP)*; IEEE, 2017; pp 469−475.
(53) Brockmann, W.*Klebtechnik: Klebstoffe, Anwendungen und Verfahren*; John Wiley & Sons, 2005.
(54) Wu, L.; Hoa, S. V.; Minh-Tan; Ton-That. Effects of the composition of hardener on the curing and aging for an epoxy resin system. *J. Appl. Polym. Sci.* **2006**, *99*, 580−588.
(55) Carfagna, C.; Apicella, A.; Nicolais, L. The effect of the prepolymer composition of amino-hardened epoxy resins on the water sorption behavior and plasticization. *J. Appl. Polym. Sci.* **1982**, *27*, 105−112.
(56) ASTM. *D5229/D5229M-04. Standard Test Method for Moisture Absorption*, 2004.
(57) Balar, N. L.*Thermomechanical Behavior of Semiconducting Polymers*; North Carolina State University, 2019.
(58) Krupka, J. Precise measurements of the complex permittivity of dielectric materials at microwave frequencies. *Mater. Chem. Phys.* **2003**, *79*, 195−198.
(59) Idolor, O.; Guha, R. D.; Berkowitz, K.; Grace, L. An experimental study of the dynamic molecular state of transient moisture in damaged polymer composites. *Polym. Compos.* **2021**, *42*, 3391.
(60) Berkowitz, K.; Guha, R. D.; Idolor, O.; Pankow, M.; Grace, L.Impact Damage Detection Limits of Microwave NDE Technique for Polymer Composites. *Proceedings of the American Society for Composites—Thirty-Sixth Technical Conference on Composite Materials*; National Science Foundation, 2021.
(61) Bermejo, J. S.; Ugarte, C. M. Influence of Cross-Linking Density on the Glass Transition and Structure of Chemically Cross-Linked PVA: A Molecular Dynamics Study. *Macromol. Theory Simul.* **2009**, *18*, 317−327.
(62) Sharaf, M. A.; Mark, J. E. The effects of cross-linking and strain on the glass transition temperature of a polymer network. *Rubber Chem. Technol.* **1980**, *53*, 982−987.
(63) Huang, J.; Romero-Torres, S.; Moshgbar, M.Practical Considerations in Data Pre-treatment for NIR and Raman Spectroscopy, American Pharmaceutical Review. 2010. Dostopno na: http://www.americanpharmaceuticalreview.com/Featured-Articles/116330-Practical-Considerations-in-Data-Pre-treatment-for-NIR-and-Raman-Spectroscopy/.(accessed Sept 10, 2019).
(64) Fornés, V.; Chaussidon, J. An interpretation of the evolution with temperature of the $\nu 2+\nu 3$ combination band in water. *J. Chem. Phys.* **1978**, *68*, 4667−4671.
(65) Musto, P.*Epoxy-bismaleimide Systems: Network Development and Structure, and Effect of These on Water Interactions and Thermal-Oxidative Stability*; Loughborough University, 2000.
(66) Buijs, K.; Choppin, G. R. Near-Infrared Studies of the Structure of Water. I. Pure Water. *J. Chem. Phys.* **1963**, *39*, 2035−2041.
(67) Singh, T. B.; Rey, L.; Gartia, R. K.*Applications of PeakFit Software in Thermoluminescence Studies*; NISCAIR-CSIR, 2011.
(68) Fan, X.Mechanics of moisture for polymers: fundamental concepts and model study. *EuroSimE 2008-International Conference on*

https://doi.org/10.1021/acsapm.2c01570
ACS Appl. Polym. Mater. 2023, 5, 400−411

Thermal, Mechanical and Multi-Physics Simulation and Experiments in Microelectronics and Micro-systems; IEEE, 2008; pp 1−14.
(69) Tsai, Y. I.; Bosze, E. J.; Barjasteh, E.; Nutt, S. R. Influence of hygrothermal environment on thermal and mechanical properties of carbon fiber/fiberglass hybrid composites. *Compos. Sci. Technol.* **2009**, *69*, 432−437.

https://doi.org/10.1021/acsapm.2c01570
ACS Appl. Polym. Mater. 2023, 5, 400−411